Lithium isotope behaviour during weathering in the Ganges alluvial plain

Philip A.E. Pogge von Strandmann[1*], Patrick J. Frings[2,3], Melissa J. Murphy[4]

[1]London Geochemistry and Isotope centre (LOGIC), Institute of Earth and Planetary Sciences, University College London and Birkbeck, University of London, Gower Street, London, WC1E 6BT, UK.

[2]Earth Surface Geochemistry, Helmholtz Centre Potsdam, GFZ German Research Centre for Geosciences, Telegraphenberg, 14473 Potsdam, Germany.

[3]Department of Geoscience, Swedish Museum of Natural History, 10405 Stockholm, Sweden.

[4]Department of Earth Sciences, Oxford University, South Parks Road, Oxford, OX1 3AN, UK.

*Corresponding author: p.strandmann@ucl.ac.uk

Abstract

The Ganges river system is responsible for the transportation of a large flux of dissolved materials derived from Himalayan weathering to the oceans. Silicate weathering-driven cooling resulting from uplift of the Himalayas has been proposed to be a key player in Cenozoic climate variation. This study has analysed Li isotope (δ^7Li) ratios from over 50 Ganges river waters and sediments, in order to trace silicate weathering processes. Sediments have δ^7Li of ~0‰, identical to bulk continental crust, however suspended sediment depth profiles do not display variations associated with grain size that have been

observed in other large river systems. Dissolved δ^7Li are low (~11‰) in the Ganges headwaters, but reach a constant value of 21 ± 1.6‰ within a relatively short distance downstream, which is then maintained for almost 2000 km to the Ganges mouth. Given that Li isotopes are controlled by the ratio of primary mineral dissolution to secondary mineral formation, this suggests that the Ganges floodplain is at steady-state in terms of these processes for most of its length. Low δ^7Li in the mountainous regions suggest silicate weathering is therefore at its most congruent where uplift and fresh silicate exposure rates are high. However, there is no correlation between δ^7Li and the silicate weathering rate in these rivers, suggesting that Li isotopes cannot be used as a weathering-rate tracer, although they do inform on weathering congruency and intensity. The close-to-constant δ^7Li values for the final 2000 km of Ganges flow also suggest that once the size of the alluvial plain reached more than ~500 km (the flow distance after which riverine δ^7Li stops varying), the Ganges exerted little influence on the changing Cenozoic seawater δ^7Li, because riverine δ^7Li attained a near steady-state composition.

1.0 Introduction

Chemical weathering of silicate rocks is a significant long-term removal process of atmospheric CO_2, both through supply of cations and alkalinity for marine carbonate precipitation, and through supply of nutrients for organic carbon burial (Berner, 2003; Berner et al., 1983; Walker et al., 1981; West et al., 2002; West et al., 2005). As such, it has long been postulated as a key long-term climate control and stabilisation mechanism. In the Cenozoic, in particular, it is

questioned whether the observed ~40 Myr cooling trend and CO_2 decline were caused by uplift of the Himalayas, which increased the supply of primary material for weathering, which in turn removed more atmospheric CO_2 (Raymo, 1994; Raymo and Ruddiman, 1992; Raymo et al., 1988). The question of whether tectonic processes can strongly affect CO_2 drawdown is critical for understanding the Earth's climate system, because it may suggest that a temperature-driven stabilising feedback on CO_2 via weathering (the Earth's "weathering thermostat") is at times a relatively weak control on climate compared to a supply-driven or organic carbon-driven control (Gíslason et al., 2006; Gislason et al., 2009; Maher and Chamberlain, 2014; Oelkers et al., 2012; West, 2012).

Evidence for the controls on weathering initially focussed on marine Sr isotope ratios, which started to increase approximately 40 Ma ago (McArthur et al., 2001). This increase was interpreted as a greater input of radiogenic continental material, implying greater weathering and CO_2 drawdown, likely due to Himalayan uplift. However, it has since become clear that the interpretation of the $^{87}Sr/^{86}Sr$ curve is not straightforward, because of the effect of metamorphosed radiogenic Himalayan carbonates (Bickle et al., 2005; Galy et al., 1999; Oliver et al., 2003; Palmer and Edmond, 1992). It is therefore not clear how much of the increase in seawater $^{87}Sr/^{86}Sr$ is due to weathering of continental silicates, and how much due to metamorphosed carbonates (Galy et al., 1999), the latter of which would not affect atmospheric CO_2 on timescales >~10,000 years, and may even be a source of CO_2, if the dominant source of acidity is sulphuric acid (Torres et al., 2014). Equally, seawater osmium isotopes show a punctuated increase from ~60 Ma (Peucker-Ehrenbrink and Ravizza,

2000; Peucker-Ehrenbrink et al., 1995), and here debate has focussed on the control radiogenic black shales in Himalayan lithologies may exert on seawater $^{187}Os/^{188}Os$ ratios (Pierson-Wickmann et al., 2002a, b). Hence, both of the above radiogenic isotope systems can at best only provide somewhat ambiguous interpretations as to whether weathering rates, or rock weatherability, increased due to the Himalayas, because of the effect of individual Sr- and Os-rich lithologies.

More recently, lithium isotopes have been used to try to answer this question. Seawater δ^7Li appears to have started increasing between 50 and 60 Ma, with behaviour more similar to Os than Sr isotope records (Hathorne and James, 2006; Misra and Froelich, 2012). As a stable isotope system, Li is virtually unaffected by the lithologies undergoing weathering, and is isotopically fractionated by the weathering process. Specifically, Li in rocks is overwhelmingly dominated by the silicate fraction, meaning that Li isotopes are probably the only proxy that solely traces silicate weathering (Kisakürek et al., 2005; Millot et al., 2010). The Li isotope ratio of silicate rocks describes a very narrow range ($\delta^7Li_{continental\ crust} \sim 0.6 \pm 0.6‰$ (Sauzeat et al., 2015; Teng et al., 2004); $\delta^7Li_{basalt} = \sim 3–5‰$ (Elliott et al., 2006; Tomascak et al., 2008)), relative to that reported in river waters ($\delta^7Li = 2–44‰$; global mean 23‰ (Bagard et al., 2015; Dellinger et al., 2014; Henchiri et al., 2016; Huh et al., 2001; Huh et al., 1998; Kisakürek et al., 2005; Liu et al., 2015; Millot et al., 2010; Pogge von Strandmann et al., 2010; Pogge von Strandmann et al., 2006; Pogge von Strandmann and Henderson, 2015; Rad et al., 2013; Vigier et al., 2009; Wang et al., 2015; Wimpenny et al., 2010b; Witherow et al., 2010). This high variability in rivers is caused by weathering processes: dissolution of silicates causes no

101 isotope fractionation, but secondary minerals formed during weathering
102 preferentially take up ^{6}Li, driving residual waters isotopically heavy (Huh et al.,
103 2001; Pistiner and Henderson, 2003; Pogge von Strandmann et al., 2010; Vigier
104 et al., 2008; Wimpenny et al., 2010a). Therefore, surface water $\delta^{7}Li$ is controlled
105 by the ratio of primary mineral dissolution (low $\delta^{7}Li$, high [Li]) relative to
106 secondary mineral formation (driving waters to high $\delta^{7}Li$, and low [Li]). This
107 ratio has also been described as the weathering congruency (Misra and Froelich,
108 2012; Pogge von Strandmann et al., 2013), weathering efficiency (Pogge von
109 Strandmann and Henderson, 2015) or weathering intensity (Dellinger et al.,
110 2015; Pogge von Strandmann et al., 2010). When riverine $\delta^{7}Li$ = rock $\delta^{7}Li$, then
111 weathering is congruent (water chemistry = rock chemistry), efficient (cations
112 are not retained in clays, but are delivered to the oceans) and low intensity (little
113 clay formation, and a low weathering to denudation ratio – bearing in mind that
114 "weathering intensity" has been defined differently by different authors).
115 If, as seems likely, the ~9‰ increase from early Cenozoic seawater to
116 the present day was controlled by changes in weathering rates or processes, it
117 would imply an increasing relative proportion of secondary mineral formation
118 (Bouchez et al., 2013; Li and West, 2014; Misra and Froelich, 2012; Vigier and
119 Godderis, 2015; Wanner et al., 2014). Initially, this was interpreted as directly
120 due to mountain uplift (Misra and Froelich, 2012). However, High Himalayan
121 rivers tend to have low $\delta^{7}Li$ values suggesting little clay formation (Kisakürek et
122 al., 2005), and in general uplifting and denuding terrains tend to have lower $\delta^{7}Li$
123 than flatter terrains, because of the continuous exposure of isotopically light
124 primary rock, and lower rock-water interaction times in the former, and longer
125 water-rock interaction times leading to greater precipitation of secondary

minerals in the low-lying areas (Dellinger et al., 2015; Pogge von Strandmann and Henderson, 2015). This has led to the proposal that the seawater δ^7Li curve is charting the evolution of the Himalayan floodplains (or others, such as those of the Andes), rather than the mountain uplift and exposure itself (Pogge von Strandmann and Henderson, 2015). This also agrees with the concept that more CO_2 is drawn down in these floodplains, rather than in the mountains (Lupker et al., 2012; West et al., 2002).

Therefore, studies have begun examining the Ganges-Brahmaputra floodplains to examine weathering and Li behaviour in low-lying floodplain settings. Sample sets taken ~10 years apart (in the late 1980s and late 1990s) from Rishikesh in the Ganges headwaters have lower δ^7Li than samples taken close to the river mouth (Bagard et al., 2015; Huh et al., 1998). To date, the highest sample resolution is from Bagard et al. (2015), which comprises four samples along the ~2500 km of the Ganges, with δ^7Li increasing from ~10 to 24‰.

This study has increased this sample resolution by an order of magnitude, with an average sample spacing of ~50 km along the Ganges and its tributaries, using samples that have previously been analysed for silicon isotopes (Frings et al., 2015). We have also analysed the Li isotope composition of a series of sediments and suspended load material from various parts of the Ganges plain, which has not previously been attempted in this region. In combination with published data from the High Himalayas, and the above-mentioned low sample-resolution studies, we provide an insight into how the Ganges-Brahmaputra floodplain affects Li isotope signals discharging into the ocean, and

150 what this tells us about modern floodplain weathering and global weathering
151 signals in the geological past.
152
153 2.0 Samples
154 The study area and samples are described by Frings et al. (2015), and
155 focus on the Ganges Alluvial Plain. Briefly, the Ganges (Fig. 1) drains a basin of
156 ~0.98 × 10^6 km^2 and has a mean annual discharge in Bangladesh of ~490 × 10^9
157 m^3 yr^{-1}. The drainage area covers the Himalayas to the north, the hills of the
158 Indian peninsular to the south, and the Ganges Alluvial Plain between them (Fig.
159 1). 80% of water in the drainage area is provided during the summer monsoon.
160 Sampling occurred at the end of the peak flood, in September 2013, and samples
161 were taken from 51 locations from tributaries around Rishikesh in NW India, at
162 the base of the Himalayas, along the Ganges and tributaries, to Farrakah, which is
163 where the Ganges distributary system begins. A further sample was taken close
164 to Calcutta, along the Hooghly River, which is one of these distributaries draining
165 into the Bay of Bengal. Overall the Ganges Basin has been extensively studied for
166 weathering processes, with a particular emphasis on the Himalayan portion of
167 the system (Bickle et al., 2005; Dalai et al., 2002; Galy and France-Lanord, 1999;
168 Galy et al., 1999; Rai et al., 2010).
169
170 3.0 Methods
171 Samples were collected in 2013 as detailed by Frings et al. (2015). At
172 most locations, water depth was determined with a ballasted sounding line, and
173 5 litres of water collected at the surface, at maximum depth, and at the centre
174 point using a horizontal van Dorn style water sampler. This was filtered at 0.4

μm within a few hours using a Teflon-coated pressure filtration system. The filters were retained, freeze-dried and the sediment gently removed from the filter.

Anion concentrations were measured by ion chromatography at the Department of Biology, Lund University, while major and minor cations, including Li, were measured by ICP-OES and ICP-MS, respectively, at University College London. The precision of these measurements is <±5% (Frings et al., 2015). Sediments and rock standards were dissolved in steps of HF-HNO_3, followed by HNO_3 and HCl.

For Li isotope analysis, sufficient sample was dried down to attain ~20ng of Li, and passed through a two-step cation exchange chromatography (AG50W X-12), using dilute HCl as an eluent. Isotopic analyses were conducted on a Nu Instruments HR multi-collector ICP-MS, relative to the standard L-SVEC (Flesch et al., 1973), at the Department of Earth Sciences, Oxford University. The exact methods for chemistry and analysis are detailed elsewhere (Pogge von Strandmann et al., 2011; Pogge von Strandmann and Henderson, 2015; Pogge von Strandmann et al., 2013). Seawater was run as an "unknown" standard, yielding δ^7Li = 31.3 ± 0.6‰ (2sd, n=48, column passes=48) over a three-year period. Two rock standards were also run, granite JG-2 (δ^7Li = 0.4 ± 0.2‰, n=3) and Wyoming oil shale SGR-1b (δ^7Li = 3.6 ± 0.4‰, n=3), where results are within uncertainty of other published values (Jeffcoate et al., 2004; Phan et al., 2016; Vigier et al., 2008; Wunder et al., 2006). The total procedural blank of this method was effectively undetectable (<0.005ng Li), which is insignificant relative to the 10–20 ng of Li analysed in each sample.

4.0 Results

Overall, the sampled rivers exhibit a standard positive trend between Ca/Na and Mg/Na (not shown), and exhibit a broadly similar range to that displayed by global rivers (Gaillardet et al., 1999b). Most samples are closer to the lower, silicate, end-member.

Lithium concentrations in the river waters vary between 0.4 and 11.7 ng/ml (Table 1). This is a similar range to other large multi-lithology rivers systems that have been studied, such as the Mackenzie River (Millot et al., 2010) and the Amazon (Dellinger et al., 2015). Highest [Li] in these river samples are in the Yamuna River, but concentrations decrease in the Yamuna before it joins the Ganges, and therefore at the confluence of the two rivers, [Li] in both is broadly similar. Lowest [Li] occurs in the Ganges at the base of the Himalayas, and also in all rivers within ~1000km of the river mouth, within the lower reaches of the alluvial plain (Fig. 2a).

Li isotope ratios range between 10.7 and 24.8‰, with the bulk of the data clustered in a relatively narrow band between 19 and 22‰. This is a narrower range than the Mackenzie and Amazon river systems overall (9–29‰ and 1.2–33‰, respectively), but greater than the Mackenzie lowland regions (10–17‰) (Dellinger et al., 2015; Millot et al., 2010). The Ganges itself has the lowest δ^7Li in the Himalayan foothills (10.7–12.9‰; Fig. 2b). At a similar distance upstream, the Yamuna has a much higher δ^7Li (18–22‰), highlighting the difference between alluvial plain and foothills weathering. From ~2000km upstream of the river mouth, δ^7Li values are fairly constant at δ^7Li = 21 ± 1.6‰. Thus, rivers wholly draining the alluvial plain have virtually identical δ^7Li to the downstream Ganges. Unlike data reported from the Congo (Henchiri et al., 2016), Li data from

225 the Ganges do not appear represent simple two-endmember mixing, but imply
226 isotope fractionation processes occurring during weathering (Section 5.1).
227 River sediment Li isotope ratios range from -2.6 to 2.9‰, with an average
228 δ^7Li of -0.3 ± 1.3‰ (Table 2), which is within uncertainty of the value of the
229 upper continental crust (Sauzeat et al., 2015; Teng et al., 2004), although they
230 exhibit a larger range than values of -1.02 to +0.39‰ reported from a single
231 location close to the mouth of the Ganges (Dellinger et al., 2014). Given that
232 rivers such as the Amazon have displayed depth-trends in Li isotope
233 composition, with decreasing δ7Li values with increasing grain size (Dellinger et
234 al., 2014), this study analysed δ^7Li values from sediments at different depths in
235 several locations, as well as from a bank deposit. No trend with depth exists in
236 these rivers, implying that the suspended load is better mixed, or has a more
237 consistent mineralogy, than in the Amazon. Overall the 4.5‰ range in sediment
238 isotope ratios over ~2000 km of river flow (Fig. 3) is similar to the 5‰ range in
239 the Mackenzie River basin (Millot et al., 2010), but smaller than the 9‰ range
240 reported from the Amazon (Dellinger et al., 2014).
241
242 5.0 Discussion
243 Lithium isotopes provide information on the balance of silicate rock
244 dissolution to secondary mineral formation, described as the weathering
245 congruency, or the weathering intensity. It is important to note that different
246 studies define "weathering intensity" in different ways, such that high
247 weathering intensity has been considered as high primary rock dissolution and
248 low dissolved δ^7Li (Kisakürek et al., 2005; Pogge von Strandmann et al., 2010;
249 Pogge von Strandmann et al., 2013), while in other studies it is considered as

high secondary mineral formation and high dissolved δ^7Li (Dellinger et al., 2015). In this study we adopt the terminology of Dellinger et al., 2015, while noting that yet other definitions are also available (Millot et al., 2010). All of these studies however agree that high secondary mineral formation relative to primary mineral dissolution drives dissolved δ^7Li high.

5.1 Comparison of lithium isotopes to river chemistry

It has been demonstrated that Li isotopes are not affected by dissolution of carbonates, both in the High Himalayas (Kisakürek et al., 2005) and in the Mackenzie catchments (Millot et al., 2010), but are solely controlled by silicate weathering. Mixing relationships (e.g. between Ca/Na and Li/Ca) that were used in those studies to show this are not as apparent in the Ganges, possibly because secondary processes are affecting both [Ca] (e.g. plant growth/decay) and [Li] (e.g. secondary mineral destabilisation), as well as effects by the dissolution of evaporites on Na and possibly Li (Galy and France-Lanord, 1999; Rai et al., 2010). Nevertheless, it is clear that riverine δ^7Li values are not being controlled by carbonate weathering, because samples with highest Ca/Na have low δ^7Li, while carbonates tend to have isotopically heavy, seawater-like, values (Lechler et al., 2015; Marriott et al., 2004; Pogge von Strandmann et al., 2013).

In a number of river studies, Li/Na ratios have been reported to have similar behaviour to Li isotope ratios, and the former has been inferred as a tracer of water-rock interaction time (Dellinger et al., 2015; Liu et al., 2015; Millot et al., 2010). This is because Na is thought to be significantly more mobile than Li during weathering, and, generally, little Na is incorporated into secondary minerals compared to Li. Waters with lowest δ^7Li have highest Li/Na,

275 defining a negative co-variation and thus agreeing with the trend shown in other
276 studies (Bagard et al., 2015; Dellinger et al., 2015; Liu et al., 2015; Millot et al.,
277 2010). However, in these Ganges waters, there is significant variation (over an
278 order of magnitude) in Li/Na for a virtually constant δ^7Li (Fig. 4). This suggests a
279 degree of decoupling between [Li] and δ^7Li in these waters, which is also
280 observed in the lack of direct co-variation between these two parameters.
281 Interestingly, data from the High Himalayas (Kisakürek et al., 2005) exhibit a
282 similar pattern (Fig. 4), with relatively constant δ^7Li for a high variation in Li/Na
283 (~0.0001 to 0.001). Although the data are sparser, the same could be argued for
284 the Ganges-Brahmaputra study of Bagard et al. (2015).
285 Overall, some of the data from global rivers show a logarithmic
286 relationship between δ^7Li and Li/Na, apparently consistent with kinetic
287 fractionation, and possible to simulate with a Rayleigh equation. Given that much
288 of river weathering is an open system, riverine behaviour should not be able to
289 be attributed to closed-system Rayleigh behaviour, and we also examine
290 equilibrium fractionation processes. To assess Rayleigh fractionation factors we
291 use a standard approach used by a number of studies (Bagard et al., 2015;
292 Dellinger et al., 2015; Pogge von Strandmann et al., 2012), but in this case we use
293 an average continental crust δ^7Li of 0‰ as the initial composition, assuming
294 entirely congruent weathering. There is significant scatter, most likely due to
295 lithology effects on Li/Na ratios (for example, due to a range of initial Li/Na
296 compositions or due to the formation of Na-bearing secondary minerals, such as
297 zeolites (e.g. analcime, chabazite, phillipsite, etc.), or smectites such as Na-
298 montmorillonite), and similar effects on δ^7Li, because primary lithology will
299 determine secondary mineralogy, which will affect Li isotope fractionation

300 factors (Millot and Girard, 2007; Pistiner and Henderson, 2003; Pogge von
301 Strandmann et al., 2010; Pogge von Strandmann et al., 2006; Vigier et al., 2008;
302 Williams and Hervig, 2005). It is possible that in rivers draining multiple
303 lithologies, though, less concentrated terrains (such as basaltic ones) do not
304 contribute enough Li to affect fractionation. For example, the Chambal
305 tributaries to the Yamuna have similar δ^7Li and [Li] values, despite also draining
306 basalts (Lupker et al., 2012). However, a best-fit Li isotope Rayleigh fractionation
307 factor for global data (Fig. 4) is $\alpha \sim 0.995$ (Δ^7Li = -5‰), as also suggested for the
308 Ganges-Brahmaputra (Bagard et al., 2015). Maximum and minimum
309 fractionation factors, which incorporate the totality of the data (excluding
310 Amazonian samples that are controlled by secondary mineral re-dissolution
311 (Dellinger et al., 2015)) are $\alpha = 0.985$ (Δ^7Li = -15‰) and $\alpha = 0.9975$ (Δ^7Li = -
312 2.5‰). As mentioned above, it is notable that almost all of the High Himalayan
313 data (Kisakürek et al., 2005) and the Ganges data from this study plot above the
314 median $\alpha = 0.995$ line. This study's Ganges samples are encompassed by
315 fractionation factors of 0.9955 – 0.985, although when precipitation corrected
316 Li/Na* ratios are used (using the correction detailed by Frings et al., 2015, using
317 the methods of other Ganges studies (Bickle et al., 2005; Dalai et al., 2002; Galy
318 and France-Lanord, 1999; Galy et al., 1999; Rai et al., 2010)), this changes slightly
319 to 0.995–0.98, with a median fractionation factor of 0.988 (Δ^7Li = -13‰). Other
320 large rivers like the Amazon also plot above the 0.995 line, where their starting
321 compositions are similar to those of the Ganges (Dellinger et al., 2014).
322 Generally, sediments from these rivers exhibit a similar range in Li/Na to each
323 other and to global shales (Fig. 4). In contrast, rivers that drain basaltic terrains
324 (Iceland, Azores, Columbia River Basalts (Liu et al., 2015; Pogge von Strandmann

et al., 2010; Pogge von Strandmann et al., 2006) do have a significantly different starting Li/Na (Fig. 4), although the effect of using a basaltic starting δ^7Li composition of 3–5‰ higher than the continental crust is relatively minor.

Whereas basaltic data follow a Rayleigh relationship (Fig. 4), this study's Ganges data appear to be closer to an equilibrium (batch) relationship (dashed lines in Fig. 4), mostly plotting between fractionation factors of 0.97–0.98. Such a relationship implies that the Ganges reaches a steady-state between primary rock dissolution and secondary mineral formation (this is discussed in more detail in Section 5.2), whereas the supply-rich (i.e. kinetically-limited) basaltic terrains and High Himalayas do not.

Generally, then, weathering of large continental crust floodplains such as that of the Ganges appears to cause an equilibrium-style relationship, requiring higher Li isotope fractionation factors than basaltic terrains. This is likely due to the different types of secondary mineral that form in different weathering environments. For example, kaolinites, which tend to be associated with weathering of intermediate to felsic continental crust rather than basalt, are thought to impart relatively high Li isotope fractionation factors (Millot and Girard, 2007; Pistiner and Henderson, 2003). There therefore appears to be some degree of lithological control over Li isotope ratios in rivers in general, because the primary lithology will control secondary mineralogy, and hence the fractionation factors it imposes (Pogge von Strandmann et al., 2010; Wang et al., 2015). This means, for example, that the interpretation of Li isotopes as a palaeo-weathering proxy (Hathorne and James, 2006; Lechler et al., 2015; Misra and Froelich, 2012; Pogge von Strandmann et al., 2013; Ullmann et al., 2013) requires

some knowledge of the weathered lithology to make quantitative interpretations about the weathering fluxes.

Using the median fractionation factors described above for the Ganges, the same distillation relationships can be used to describe the fraction of Li in solution, relative to that in the solid phase (Frings et al., 2015; Millot et al., 2010; Pogge von Strandmann et al., 2012; Vigier et al., 2009). Hence, if the δ^7Li of a river were 0‰, identical to the source rocks, 100% of Li would be in solution. For Rayleigh fractionation (median α = 0.988), on average 19% of Li is in solution (2–37% for the full range of α), while this number is 20% for equilibrium fractionation (median α = 0.975). Frings et al. (2015) determined catchment areas and estimated river fluxes to give the yield of major elements. For Si, they then divided this yield by the fraction of Si in solution, determined from Si isotope ratios using a Rayleigh relationship, to give the initial Si mobilisation rate, independent of secondary mineral formation. This determined that ~75% of Si mobilisation in the Ganges occurs outside the Himalayas, in the alluvial plain and peninsular rivers.

Here, we perform the same type of calculation for Li, which shows that around 63% of initial Li mobilisation (total ~12 Gmol/yr Li if Rayleigh, ~1.1 Gmol/yr if equilibrium) occurs outside the Himalayas. This percentage is highly insensitive to the fractionation factor used (the entire range in α for these Ganges samples changes this percentage by 0.6%). This therefore shows that greater silicate weathering occurs away from the mountain areas, which agrees with estimates based on bulk chemistry (West et al., 2002), and Li isotope studies from New Zealand (Pogge von Strandmann and Henderson, 2015), as well as reactive-flow modelling (Bouchez et al., 2013). However, there is a

difference in the estimates based on Si isotopes (~25% of initial Si is from the Himalayas (Frings et al., 2015)), with those based on Li isotopes (~38% of initial Li is from the Himalayas, where the isotopic analytical uncertainty does not resolvably affect the final calculations). No analyses are available of Li concentrations of a broad range of sediments of the Ganges floodplain, and therefore approximate Ca or Mg fluxes based on Li isotopes cannot be calculated. The difference between Li and Si isotopes as a tracer is discussed below, but it is probable that the difference in estimates is due to different mobilities in the weathering environment. While Li and Si are similarly mobile during basalt weathering (Pogge von Strandmann et al., 2016), the complex environment of floodplains such as that of the Ganges, and the general lack of Li concentration analyses, means that such estimates are not possible yet for these terrains. In addition, some degree of control by biology over Si isotopes and concentrations is likely - in particular, due to the intensive agriculture of the Ganges alluvial plain. In contrast, Li isotopes are unlikely to be directly affected by enhanced plant growth (Clergue et al., 2015; Lemarchand et al., 2010; Pogge von Strandmann et al., 2016), and fertilisers in the High Himalayan region are thought to have higher δ^7Li than any samples observed here (Kisakürek et al., 2005).

5.2 Comparison of lithium isotopes to physical parameters

The samples furthest up the Ganges and its catchment were taken above the town of Rishikesh, almost 2500 km from the river mouth, and located in the Himalayan foothills. Lithium concentrations are relatively low here (2–3 ng/ml), but increase sharply several hundred km downstream (Fig. 2a), apparently when

399 highly concentrated tributaries from the north (with up to ~12 ng/ml Li) merge
400 with the Ganges. One of the largest tributaries, the Yamuna River, also has
401 relatively high [Li], and this also appears to serve to keep the Ganges [Li] high.
402 After the confluence of the Yamuna with the Ganges ~1500 km above the river
403 mouth, Li concentrations start to decline, and after the Ganges enters the
404 southern alluvial plain, [Li] is lower than in the Himalayan foothills. This decline
405 in concentration again appears to be driven by the tributaries in the alluvial
406 plain, which have low Li concentrations. Enhanced secondary mineral formation
407 is unlikely to be causing this concentration decline, because Li isotope ratios are
408 not being changed by whatever process is causing the concentration decrease.
409 The change in [Li] is more likely a result of dilution by precipitation-sourced
410 waters, as other elemental concentrations are also affected. However, dissolved
411 [Li] does not directly co-vary with discharge values, although it must be noted
412 that these are literature compilations rather than direct snapshot values (Frings
413 et al., 2015; Jain et al., 2007). There is a co-variation between discharge and [Li]
414 in the final ~400km, but not before (Fig. 5), suggesting that dilution is not a big
415 effect on Li concentrations aside from this final part of the Ganges (and that δ^7Li
416 is not affected by this dilution). Such a relationship is opposite to that reported
417 from the Congo (Henchiri et al., 2016).
418 In contrast, Li isotope ratios exhibit their largest variation in the
419 headwaters of the Ganges. Including this study, the river at Rishikesh has been
420 sampled for Li isotopes approximately every decade for the last 30 years (Bagard
421 et al., 2015; Huh et al., 1998), and has had uniformly low δ^7Li values of ~10–
422 13‰. In comparison, samples taken 1500–2000 km further downstream by all
423 three studies are consistently isotopically heavier, with δ^7Li ~20–23‰.

Figure 6a summarises all Li isotope studies of rivers associated with the Ganges as a function of distance from the Main Frontal Thrust (MFT), which delineates the uplifting areas from the floodplain (Huang et al., 2015). Data from the High Himalayas (Kisakurek et al., 2005), which eventually drain into the Ganges, generally have lower δ^7Li than the Ganges mainstream. In these data, rivers with lower [Li] have higher δ^7Li, so that High Himalayan rivers with high δ^7Li have little overall influence on the composition of waters downstream. The general relationship with distance clearly shows that only relatively low δ^7Li values are from the Himalayan foothills or mountains. Interestingly, the three studies of the Ganges mainstream were sampled at different time periods, i.e. those of Bagard et al. (2015) represent a low flow period, while this study represents the end of peak flooding. Nevertheless, samples from the same location are similar, implying that hydrological regime does not resolvably affect Li behaviour.

After a distance of ~500 km of flow, δ^7Li values are relatively constant, and both the Ganges and its tributaries are close to the global riverine mean of ~23‰ (Huh et al., 1998). Such constant δ^7Li values for such a long distance imply a balance between mineral dissolution and precipitation, as would be thought to characterise a floodplain at steady-state, i.e. one that maintains an approximately constant level of weathering intensity. Our data suggest that the Ganges floodplain is broadly in steady-state for ~80% of its flow length, from the area of Kanpur to the river mouth (Fig. 1 & 2b), and that weathering is only out of balance in the foothills regions of the studied area.

Pogge von Strandmann and Henderson (2015) and Dellinger et al. (2015) have both showed that Li isotope ratios in rivers tend to be driven lower in regions of higher uplift and therefore higher denudation and exposure rates,

449 because more fresh primary rock is being made available for dissolution, relative
450 to the formation of secondary minerals. In contrast, in flatter regions where
451 uplift and exposure are low (i.e. floodplains), secondary mineral formation
452 becomes relatively greater, and riverine δ^7Li values increase. These studies are
453 also backed up by the observation that rivers in the High Himalayas generally
454 have δ^7Li values lower than the global mean (Huh et al., 1998; Kisakürek et al.,
455 2005), or indeed lower than values in rivers on the floodplain at the same
456 distance from the river mouth, as shown by comparing the floodplain-based
457 Yamuna and the foothills-sourced Ganges Rivers (Fig. 2b).
458 While uplift rates are not available for these samples, in the Himalayan
459 region, altitude is an approximate facsimile to exposure. Figure 6b shows a
460 literature compilation of Li isotopes in the Ganges-Brahmaputra catchment area,
461 and there is a broad co-variation where lower altitude corresponds to higher
462 dissolved δ^7Li. There is considerable variation in the High Himalayas (Kisakürek
463 et al., 2005), which may be because very small streams are also represented in
464 that study, but as described above, rivers with lower δ^7Li will have the greater
465 influence on riverine signals downstream. Overall, however, it is probable that
466 the low δ^7Li values observed in the Ganges headwaters are due to relatively
467 greater primary rock exposure and dissolution (more congruent silicate
468 weathering), while the increase in δ^7Li further downstream is due to increasing
469 secondary mineral formation (more incongruent silicate weathering), due to
470 increased water-rock interaction times (reaction kinetics) driving a greater
471 degree of secondary mineral oversaturation and precipitation (reaction
472 thermodynamics).
473

5.3 Li isotopes as a proxy for silicate weathering rates

While Li isotopes are generally thought to be an excellent tracer of silicate weathering congruency or intensity, a number of studies have also found correlations between riverine δ^7Li and the silicate weathering rate. In particular, negative co-variations have been reported from Iceland (Vigier et al., 2009) and the Mackenzie River basin (Millot et al., 2010) (the Mackenzie River accounts for ~2% of global riverine discharge (Huh et al., 1998)). Some interpretations of palaeo δ^7Li data have been based on these two published negative relationships, and the assumption that clays and the dissolved load co-behave (Dosseto et al., 2015). Overall, however, it seems highly unlikely that δ^7Li can be used as a weathering rate tracer, unless the weathering system is extremely simple, and the secondary mineral formation rate and fractionation factor stays constant, while the primary mineral dissolution rate is then solely a function of the weathering rate.

In the case of these Ganges data, silicate weathering rates were calculated from the discharge rates, precipitation-corrected major element data and catchment areas calculated by Frings et al. (2015), using the methods demonstrated by numerous other studies, by correcting for silicate and evaporate components (Dalai et al., 2002; Gaillardet et al., 1999a; Galy and France-Lanord, 1999; Rai et al., 2010). As shown in Figure 7, there is no relationship between silicate weathering rate and δ^7Li for these samples (r^2 = 0.01). In other words, for one of the Earth's major rivers, that supplies ~3% of the global riverine Li flux (Huh et al., 1998), dissolved Li isotopes are not a tracer of the silicate weathering rate. Figure 7 also shows data from globally significant

498 rivers responsible for ~30% of the global riverine discharge (Huh et al., 1998),
499 which similarly exhibit no relationship between δ^7Li and weathering rate.
500 Hence, while some river systems show co-variations between these two
501 factors, overall it is clear that Li isotopes cannot be used as a weathering rate-
502 tracer, and therefore modelling must be used to determine any useful
503 weathering fluxes from riverine or seawater records (Bouchez et al., 2013;
504 Lechler et al., 2015; Li and West, 2014; Pogge von Strandmann et al., 2013; Pogge
505 von Strandmann et al., 2014; Vigier and Godderis, 2015; Wanner et al., 2014).
506
507 *5.4 Comparison between Li and Si isotopes*
508 Silicon isotope ratios have also been determined for these samples
509 (Frings et al., 2015). In theory, δ^{30}Si behaves similarly to δ^7Li, in that both
510 systems are used as silicate weathering tracers, where secondary minerals
511 preferentially take up light isotopes, driving river waters and seawater to
512 isotopically heavy values (De la Rocha et al., 2000; Georg et al., 2006; Georg et al.,
513 2007; Opfergelt et al., 2013; Opfergelt et al., 2009; Ziegler et al., 2005). In
514 addition, for Si isotopes, primary productivity (e.g. diatoms) and plant growth
515 exert an influence, and preferentially take up light isotopes (Opfergelt et al.,
516 2006). The Ganges's δ^{30}Si values have been interpreted similarly to Li isotopes
517 by Frings et al. (2015), i.e. controlled by silicate weathering congruency, with
518 additional, indistinguishable, effects from plants or other biological processes,
519 and have been used to determine silicate weathering fluxes (Frings et al., 2015).
520 It therefore makes sense to compare these two tracers, given their behavioural
521 similarity, but also their differences, as Si is a major structural element of both

522 primary silicate rocks and many secondary minerals, while Li is only a trace
523 element.
524 Overall, then, there is a positive co-variation between δ^7Li and δ^{30}Si (Fig.
525 8). This trend is pinned by the Ganges mainstream, which exhibits a good
526 correlation ($r^2 = 0.78$). Himalayan headwaters are isotopically light (congruent
527 weathering) for both systems. However, the Ganges tributaries show much
528 greater relative variability for Si isotopes than for Li isotopes. Thus, while the
529 Ganges mainstream makes up 80% of the total δ^7Li variation observed, it only
530 makes up 50% of the δ^{30}Si variability. This difference is likely due to differing
531 fractionation caused to both systems by secondary minerals, because Si is a
532 major structural component of many minerals, while Li is a trace element (Pogge
533 von Strandmann et al., 2012). However, this does not necessarily explain
534 relatively constant δ^7Li in samples with variable δ^{30}Si, because a given secondary
535 mineral should impose a set fractionation on both Li and Si isotopes. Differences
536 in reaction kinetics may therefore be a primary control of the difference in
537 isotope fractionation. Si may require more time to be incorporated into
538 neoformed minerals, while Li is at least partially controlled by sorption (Millot
539 and Girard, 2007; Pistiner and Henderson, 2003; Pogge von Strandmann et al.,
540 2016; Pogge von Strandmann et al., 2012). Alternatively, Si isotopes are affected
541 by plant and/or diatom growth, which may be imposing additional, and
542 potentially quite spatially variable, fractionation (Opfergelt et al., 2006; Opfergelt
543 et al., 2011), and therefore the δ^{30}Si variability beyond that which correlates with
544 Li isotopes could be a biologically-induced effect. Hence, the Ganges system, with
545 its longer water flow time in the alluvial plain compared to most rivers studied
546 for Li isotopes, would be expected to approach a state where both Li and Si

547 isotopes reach a degree of steady-state. In addition, a co-variation has also been
548 reported from plant- and organic-poor waters from Iceland (Fig. 8), suggesting
549 that in systems where biological fractionation of Si isotopes is low, Li and Si
550 isotopes will behave similarly (Opfergelt et al., 2013), because Li isotopes are
551 unaffected by plants (Lemarchand et al., 2010; Pogge von Strandmann et al.,
552 2016).
553
554 *5.5 Global implications of the Ganges Li chemistry*
555 It is clear from the comparison of Li and Si isotopes that silicate
556 weathering is more congruent (less intense) in the Himalayan foothills of the
557 Ganges than it is in the alluvial plain. It has equally been shown that on average
558 High Himalayan catchments are even more congruent (Fontorbe et al., 2013;
559 Kisakürek et al., 2005). This behaviour makes it abundantly clear that dominant
560 secondary mineral formation, and hence isotope fractionation, occurs in the
561 floodplains. This evidence is substantiated by both mineralogical analyses that
562 suggest that authigenic clays only become dominant in alluvial plains
563 (Chakrapani et al., 1995), and by other estimates of weathering by solute mass
564 balance (Galy and France-Lanord, 1999; Lupker et al., 2012; West et al., 2002),
565 which also suggest that the primary locus of CO_2 drawdown through silicate
566 weathering is in floodplains rather than steep slopes.
567 Overall, an increase in Himalayan denudation, delivered to the oceans by
568 the Ganges-Brahmaputra river system, has been argued to be the (or a) cause of
569 increases in seawater $^{87}Sr/^{86}Sr$ and $^{187}Os/^{188}Os$ (Bickle et al., 2005; Galy et al.,
570 1999; Oliver et al., 2003; Pierson-Wickmann et al., 2002a, b; Sharma et al., 1999).
571 The increase in Cenozoic seawater δ^7Li (Hathorne and James, 2006; Misra and

572 Froelich, 2012) has also been interpreted as due to increased Himalayan
573 weathering (Froelich and Misra, 2014). More recently, data from other uplift and
574 exposure sites have suggested that mountain regions themselves are only the
575 drivers of physical erosion, and that the Li isotope fractionation occurs in the
576 floodplains (Dellinger et al., 2015; Pogge von Strandmann and Henderson, 2015).
577 Interestingly, the Ganges controls the Li flux to the oceans to a similar
578 extent as it does the Sr or Os fluxes, despite the latter two systems also having
579 carbonate sources. The Ganges provides ~3% of the total riverine supply of Li to
580 the oceans (compared to 2% of Os (Levasseur et al., 1999) and ~3% of Sr
581 (Krishnaswami et al., 1992)), and the whole Ganges-Brahmaputra system ~7%
582 (Huh et al., 1998), with another estimated 2% of the total flux provided by
583 groundwater flow into the Bengal Basin (Bagard et al., 2015). Combined, the
584 three main mountain-sourced river systems with floodplains that greatly
585 increased in size during the Cenozoic (Ganges-Brahmaputra, Amazon and
586 Orinoco) provide almost 16% of the modern global Li flux from rivers to the
587 oceans, compared to an estimated ~20% for Sr (Raymo et al., 1988). The three
588 rivers mentioned above would have to increase their mean δ^7Li by 30–40‰ to
589 drive the observed seawater change at equilibrium, with no change in flux, which
590 is extremely unlikely, given observations of modern rivers. Even the evolution of
591 their floodplains (Pogge von Strandmann and Henderson, 2015) is unlikely to be
592 responsible for the entire change in seawater δ^7Li. Hence, the relationship
593 between continental weathering changes and seawater δ^7Li is not
594 straightforward, and other Cenozoic changes, such as a “sink-shift” (Li and West,
595 2014) or temperature-dependent changes in deep-ocean fractionation factors

596 (Coogan and Dosso, 2015), may have to be invoked in combination with a
597 weathering change.
598 The other inference that can made from these Ganges data for the
599 Cenozoic evolution of seawater δ^7Li is that it appears that growth of the Ganges
600 floodplain beyond ~500km from the Himalayan foothills would no longer change
601 seawater δ^7Li, as evidenced by the near constant riverine δ^7Li values. Beyond
602 this point, under present climatic conditions, the floodplain is in approximate
603 steady-state for Li isotopes (and also for Si isotopes (Frings et al., 2015)). A
604 similar observation can be made for the Amazon, where most fractionation
605 occurs close to the foothills, and then remains constant across the floodplain
606 (Dellinger et al., 2015). If present-day measurements can be used as an analogy
607 for general Cenozoic behaviour (as used for Sr isotopes (Galy et al., 1999)), then
608 the final 2000 km of Ganges flow creates no change in δ^7Li, and the evolution of
609 the floodplain beyond ~500km will not create further change in seawater δ^7Li
610 once this has reached equilibrium with regards to input.
611
612 6.0 Conclusions
613 This study has analysed Li isotopes from over 50 samples of the Ganges
614 river and its tributaries, representing over an order of magnitude increase in
615 sampling density compared to previous studies. Lithium isotope ratios are fairly
616 constant for the lower ~2000 km of flow of the Ganges, and δ^7Li only decreases
617 at the head of the river in the Himalayan foothills. Silicate weathering is
618 therefore at its most congruent in mountainous regions where uplift and fresh
619 silicate exposure rates are high. These data were used to calculate a Li yield from
620 primary rock, indicating that over 63% of Ganges Li stems from the floodplains,

621 rather than the mountainous regions. This observation agrees with those made
622 from bulk river chemistry, as well as Si isotopes, although the precise fraction of
623 Li and Si coming from the Himalayas appears to be different, based on their
624 individual isotope systems, likely due to a combination of secondary mineral
625 reaction kinetics, and the influence of biology over Si.

626 Overall, despite some publications using Li isotopes as a tracer for the
627 silicate weathering rate, there is no correlation whatsoever between Ganges δ^7Li
628 and silicate weathering rates. The lack of such a correlation in one of the Earth's
629 major rivers strongly indicates that δ^7Li also cannot be used as a direct palaeo-
630 weathering rate tracer.

631 Finally, the Li isotope data (which are controlled by the ratio of primary
632 mineral dissolution relative to secondary mineral formation) suggest that the
633 Ganges floodplains are broadly at steady-state, with dissolution and transport in
634 equilibrium. The close-to-constant δ^7Li values for the final 2000km of Ganges
635 flow also suggest that once the size of the alluvial plain reached more than ~500
636 km under present climatic conditions, the Ganges exerted little influence on the
637 changing Cenozoic seawater δ^7Li.

638

639

640 Acknowledgements

641 Analyses were supported by PPvS's NERC Advanced Research Fellowship
642 NE/I020571/2. We thank Wim Clymans for help with fieldwork, Chakrapani
643 Govind for logistical support and Will Gray for assistance with ICP-OES/MS
644 analysis. We thank Paul Tomascak, Maarten Lupker and an anonymous reviewer
645 for their insightful comments.

Bagard, M.-L., West, A.J., Newman, K. and Basu, A.K. (2015) Lithium isotope fractionation in the Ganges–Brahmaputra floodplain and implications for groundwater impact on seawater isotopic composition. Earth Planet. Sci. Lett. 432, 404–414,

Berner, R.A. (2003) The long-term carbon cycle, fossil fuels and atmospheric composition. Nature 426, 323-326,

Berner, R.A., Lasaga, A.C. and Garrels, R.M. (1983) The Carbonate-Silicate Geochemical Cycle and Its Effect on Atmospheric Carbon-Dioxide over the Past 100 Million Years. Am. J. Sci. 283, 641-683,

Bickle, M.J., Chapman, H.J., Bunbury, J., Harris, N.B.W., Fairchild, I.J., Ahman, T. and Pomies, C. (2005) Relative contributions of silicate and carbonate rocks to riverine Sr fluxes in the headwaters of the Ganges. Geochim. Cosmochim. Acta 69, 2221-2240,

Bouchez, J., von Blanckenburg, F. and Schuessler, J.A. (2013) Modeling novel stable isotope ratios in the weathering zone. Am. J. Sci. 313, 10.2475/04.2013.00I.

Chakrapani, G.J., Subramanian, V., Gibbs, R.J. and Jha, P.K. (1995) Size characteristics and mineralogy of suspended sediments of the Ganges river, India. 25, 192–196,

Clergue, C., Dellinger, M., Buss, H.L., Gaillardet, J., Benedetti, M.F. and Dessert, C. (2015) Influence of atmospheric deposits and secondary minerals on Li isotopes budget in a highly weathered catchment, Guadeloupe (Lesser Antilles). Chem. Geol. 414, 28–41,

Coogan, L.A. and Dosso, S.E. (2015) Alteration of ocean crust provides a strong temperature dependent feedback on the geological carbon cycle and is a primary driver of the Sr-isotopic composition of seawater. Earth Planet. Sci. Lett. 415, 38–46,

Dalai, T.K., Krishnaswami, S. and Sarin, M.M. (2002) Major ion chemistry in the headwaters of the Yamuna river system: Chemical weathering, its temperature dependence and CO2 consumption in the Himalaya. Geochim. Cosmochim. Acta 66, 3397–3416,

De la Rocha, C.L., Brzezinski, M.A. and DeNiro, M.J. (2000) A first look at the distribution of the stable isotopes of silicon in natural waters. Geochim. Cosmochim. Acta 64, 2467-2477,

Dellinger, M., Gaillardet, J., Bouchez, J., Calmels, D., Galy, V., Hilton, R.G., Louvat, P. and France-Lanord, C. (2014) Lithium isotopes in large rivers reveal the cannibalistic nature of modern continental weathering and erosion. Earth Planet. Sci. Lett. 401, 359–372,

Dellinger, M., Gaillardet, J., Bouchez, J., Calmels, D., Louvat, P., Dosseto, A., Gorge, C., Alanoca, L. and Maurice, L. (2015) Riverine Li isotope fractionation in the Amazon River basin controlled by the weathering regimes. Geochim. Cosmochim. Acta 164, 71–93,

Dosseto, A., Vigier, N., Joassnes-Boyau, R., Moffat, I., Singh, T. and Srivastava, P. (2015) Rapid response of silicate weathering rates to climate change in the Himalaya. Geochemical Perspectives Letters 1, 10–19,

693 Elliott, T., Thomas, A., Jeffcoate, A. and Niu, Y.L. (2006) Lithium isotope evidence
694 for subduction-enriched mantle in the source of mid-ocean-ridge basalts. Nature
695 443, 565–568,
696 Flesch, G.D., Anderson, A.R. and Svec, H.J. (1973) A secondary isotopic standard
697 for 6Li/7Li determinations. Int. J. Mass Spectrom. Ion Process. 12, 265–272,
698 Fontorbe, G., De la Rocha, C.L., Chapman, H.J. and Bickle, M.J. (2013) The silicon
699 isotopic composition of the Ganges and its tributaries. Earth Planet. Sci. Lett. 381,
700 21–30,
701 Frings, P.J., Clymans, W., Fontorbe, G., Gray, W., Chakrapani, G.J., Conley, D.J. and
702 De la Rocha, C.L. (2015) Silicate weathering in the Ganges alluvial plain. Earth
703 Planet. Sci. Lett. 427, 136–148,
704 Froelich, P.N. and Misra, S. (2014) Was the late Paleocene-early Eocene hot
705 because Earth was flat? An ocean lithium isotope view of mountain building,
706 continental weathering, carbon dioxide, and Earth's Cenozoic climate.
707 Oceanography 27, 36–49,
708 Gaillardet, J., Dupré, B. and Allègre, C.J. (1999a) Geochemistry of large river
709 suspended sediments: silicate weathering or recycling tracer? Geochim.
710 Cosmochim. Acta 63, 4037–4051,
711 Gaillardet, J., Dupre, B., Louvat, P. and Allegre, C.J. (1999b) Global silicate
712 weathering and CO_2 consumption rates deduced from the chemistry of large
713 rivers. Chem. Geol. 159, 3-30,
714 Galy, A. and France-Lanord, C. (1999) Weathering processes in the Ganges–
715 Brahmaputra basin and the riverine alkalinity budget. Chem. Geol. 159, 31–60,
716 Galy, A., France-Lanord, C. and Derry, L.A. (1999) The strontium isotopic budget
717 of Himalayan Rivers in Nepal and Bangladesh. Geochim. Cosmochim. Acta 63,
718 1905–1925,
719 Georg, R.B., Reynolds, B.C., Frank, M. and Halliday, A.N. (2006) Mechanisms
720 controlling the silicon isotopic compositions of river waters. Earth Planet. Sci.
721 Lett. 249, 290-306, 10.1016/j.epsl.2006.07.006I.
722 Georg, R.B., Reynolds, B.C., West, A.J., Burton, K.W. and Halliday, A.N. (2007)
723 Silicon isotope variations accompanying basalt weathering in Iceland. Earth
724 Planet. Sci. Lett. 261, 476-490,
725 Georg, R.B., West, A.J., Basu, A.R. and Halliday, A.N. (2009) Silicon fluxes and
726 isotope composition of direct groundwater discharge into the Bay of Bengal and
727 the effect on the global ocean silicon isotope budget. Earth Planet. Sci. Lett. 283,
728 67-74,
729 Gíslason, S.R., Oelkers, E. and Snorrason, A. (2006) Role of river-suspended
730 material in the global carbon cycle. Geology 34, 49–52,
731 Gislason, S.R., Oelkers, E.H., Eiriksdottir, E.S., Kardjilov, M.I., Gisladottir, G.,
732 Sigfusson, B., Snorrason, A., Elefsen, S., Hardardottir, J., Torssander, P. and
733 Oskarsson, N. (2009) Direct evidence of the feedback between climate and
734 weathering. Earth Planet. Sci. Lett. 277, 213-222, 10.1016/j.epsl.2008.10.018I.
735 Hathorne, E.C. and James, R.H. (2006) Temporal record of lithium in seawater: a
736 tracer for silicate weathering? Earth Planet. Sci. Lett. 246, 393–406,
737 Henchiri, S., Gaillardet, J., Dellinger, M., Bouchez, J. and Spencer, R.G.M. (2016)
738 Riverine dissolved lithium isotopic signatures in low-relief central Africa and
739 their link to weathering regimes. Geophysical Research Letters 43, 10.1002/
740 2016GL067711.I.

741 Huang, W., van Hinsbergen, D.J.J. and Kapp, P. (2015) Paleolatitudes of the
742 Tibetan Himalaya from primary and secondary magnetizations of Jurassic to
743 Lower Cretaceous sedimentary rocks. Geochem. Geophys. Geosyst.,
744 10.1002/2014GC005624I.
745 Huh, Y., Chan, L.H. and Edmond, J.M. (2001) Lithium isotopes as a probe of
746 weathering processes: Orinoco River. Earth Planet. Sci. Lett. 194, 189–199,
747 Huh, Y., Chan, L.H., Zhang, L. and Edmond, J.M. (1998) Lithium and its isotopes in
748 major world rivers: Implications for weathering and the oceanic budget.
749 Geochim. Cosmochim. Acta 62, 2039–2051,
750 Jain, S.K., Agarwal, P.K. and Singh, V.P. (2007) Hydrology and Water Resources of
751 India. Springer.
752 Jeffcoate, A.B., Elliott, T., Thomas, A. and Bouman, C. (2004) Precise, small sample
753 size determinations of lithium isotopic compositions of geological reference
754 materials and modern seawater by MC-ICP-MS. Geostandards and Geoanalytical
755 Research 28, 161-172,
756 Kisakürek, B., James, R.H. and Harris, N.B.W. (2005) Li and δ^7Li in Himalayan
757 rivers: Proxies for silicate weathering? Earth Planet. Sci. Lett. 237, 387–401,
758 Krishnaswami, S., Trivedi, J.R., Sarin, M.M., Ramesh, R. and Sharma, K.K. (1992)
759 Storntium isotopes and rubidiumin the Ganga-Brahmaputra river system:
760 Weathering in the Himalaya, fluxes to teh Bay of Bengal and contributions to the
761 evolution of oceanis 87Sr/86Sr. Earth Planet. Sci. Lett. 109, 243–253,
762 Lechler, M., Pogge von Strandmann, P.A.E., Jenkyns, H.C., Prosser, G. and Parente,
763 M. (2015) Lithium-isotope evidence for enhanced silicate weathering during OAE
764 1a (Early Aptian Selli event). Earth Planet. Sci. Lett. 432, 210–222,
765 Lemarchand, E., Chabaux, F., Vigier, N., Millot, R. and Pierret, M.C. (2010) Lithium
766 isotope systematics in a forested granitic catchment (Strengbach, Vosges
767 Mountains, France). Geochim. Cosmochim. Acta 74, 4612-4628,
768 Levasseur, S., Birck, J.L. and Allègre, C.J. (1999) The osmium riverine flux and the
769 oceanic mass balance of osmium. Earth Planet. Sci. Lett. 174, 7–23,
770 Li, G. and West, A.J. (2014) Evolution of Cenozoic seawater lithium isotopes:
771 Coupling of global denudation regime and shifting seawater sinks. Earth Planet.
772 Sci. Lett. 401, 284–293,
773 Liu, X.-M., Wanner, C., Rudnick, R.L. and McDonough, W.F. (2015) Processes
774 controlling δ7Li in rivers illuminated by study of streams and groundwaters
775 draining basalts. Earth Planet. Sci. Lett. 409, 212–224,
776 Lupker, M., France-Lanord, C., Galy, V., Lave, J., Gaillardet, J., Gajurel, A.P.,
777 Guilmette, C., Rahman, M., Singh, S.K. and Sinha, R. (2012) Predominant
778 floodplain over mountain weathering of Himalayan sediments (Ganga basin).
779 Geochim. Cosmochim. Acta 84, 410–432,
780 Maher, K. and Chamberlain, C.P. (2014) Hydrologic Regulation of Chemical
781 Weathering and the Geologic Carbon Cycle. Science 343, 1502–1504,
782 Marriott, C.S., Henderson, G.M., Crompton, R., Staubwasser, M. and Shaw, S.
783 (2004) Effect of mineralogy, salinity, and temperature on Li/Ca and Li isotope
784 composition of calcium carbonate. Chem. Geol. 212, 5–15,
785 McArthur, J.M., Howarth, R.J. and Bailey, T.R. (2001) Strontium isotope
786 stratigraphy: LOWESS version 3: Best fit to the marine Sr-isotope curve for 0-509
787 Ma and accompanying look-up table for deriving numerical age. Journal of
788 Geology 109, 155-170,

789 Millot, R. and Girard, J.P. (2007) Lithium Isotope Fractionation during adsorption
790 onto mineral surfaces, Int. meet., Clays in natural & engineered barriers for
791 radioactive waste confinement, Lille, Frace.
792 Millot, R., Vigier, N. and Gaillardet, J. (2010) Behaviour of lithium and its isotopes
793 during weathering in the Mackenzie Basin, Canada. Geochim. Cosmochim. Acta
794 74, 3897–3912,
795 Misra, S. and Froelich, P.N. (2012) Lithium Isotope History of Cenozoic Seawater:
796 Changes in Silicate Weathering and Reverse Weathering. Science 335, 818–823,
797 Oelkers, E.H., Jones, M.T., Pearce, C.R., Jeandel, C., Eiriksdottir, E.S. and Gislason,
798 S.R. (2012) Riverine particulate material dissolution in seawater and its
799 implications for the global cycles of the elements. C. R. Geosci. 344, 646–651,
800 Oliver, L., Harris, N., Bickle, M., Chapman, H., Dise, N. and Horstwood, M. (2003)
801 Silicate weathering rates decoupled from the $^{87}Sr/^{86}Sr$ ratio of the dissolved load
802 during Himalayan erosion. Chem. Geol. 201, 119–139,
803 Opfergelt, S., Burton, K.W., Pogge von Strandmann, P.A.E., Gislason, S.R. and
804 Halliday, A.N. (2013) Riverine silicon isotope variations in glaciated basaltic
805 terrains: Implications for the Si delivery to the ocean over glacial–interglacial
806 intervals. Earth Planet. Sci. Lett. 369–370, 211–219,
807 Opfergelt, S., Cardinal, D., Henriet, C., Drave, X., Andre, L. and Delvaux, B. (2006)
808 Silicon Isotopic Fractionation by Banana (Musa spp.) Grown in a Continuous
809 Nutrient Flow Device. Plant Soil 285, 333-345,
810 Opfergelt, S., de Bournonville, G., Cardinal, D., Andre, L., Delstanche, S. and
811 Delvaux, B. (2009) Impact of soil weathering degree on silicon isotopic
812 fractionation during adsorption onto iron oxides in basaltic ash soils, Cameroon.
813 Geochim. Cosmochim. Acta 73, 7226-7240,
814 Opfergelt, S., Eiriksdottir, E.S., Burton, K.W., Einarsson, A., Siebert, C., Gislason,
815 S.R. and Halliday, A.N. (2011) Quantifying the impact of freshwater diatom
816 productivity on silicon isotopes and silicon fluxes: Lake Myvatn, Iceland. Earth
817 Planet. Sci. Lett. 305, 73-82, 10.1016/j.epsl.2011.02.043I.
818 Palmer, M.R. and Edmond, J.M. (1992) Controls over the strontium isotope
819 composition of river water. Geochim. Cosmochim. Acta 56, 2099-2111,
820 Peucker-Ehrenbrink, B. and Ravizza, G. (2000) The marine osmium isotope
821 record. Terra Nova 12, 205–219,
822 Peucker-Ehrenbrink, B., Ravizza, G. and Hofmann, A.W. (1995) The Marine Os-
823 187/Os-186 Record of the Past 80-Million Years. Earth Planet. Sci. Lett. 130, 155-
824 167,
825 Phan, T.T., Capo, R.C., Stewart, B.W., Macpherson, G.L., Rowan, E.L. and Hammack,
826 R.W. (2016) Factors controlling Li concentration and isotopic composition in
827 formation waters and host rocks of Marcellus Shale, Appalachian Basin. Chem.
828 Geol. 420, 162–179,
829 Pierson-Wickmann, A.C., Reisberg, L. and France-Lanord, C. (2002a) Behavior of
830 Re and Os during low-temperature alteration: Results from Himalayan soils and
831 altered black shales. Geochim. Cosmochim. Acta 66, 1539-1548,
832 Pierson-Wickmann, A.C., Reisberg, L. and France-Lanord, C. (2002b) Impure
833 marbles of the Lesser Himalaya: another source of continental radiogenic
834 osmium. Earth Planet. Sci. Lett. 204, 203–214,
835 Pistiner, J.S. and Henderson, G.M. (2003) Lithium-isotope fractionation during
836 continental weathering processes. Earth Planet. Sci. Lett. 214, 327-339,

837 Pogge von Strandmann, P.A.E., Burton, K.W., James, R.H., van Calsteren, P. and
838 Gislason, S.R. (2010) Assessing the role of climate on uranium and lithium
839 isotope behaviour in rivers draining a basaltic terrain. Chem. Geol. 270, 227–239,
840 Pogge von Strandmann, P.A.E., Burton, K.W., James, R.H., van Calsteren, P.,
841 Gislason, S.R. and Mokadem, F. (2006) Riverine behaviour of uranium and
842 lithium isotopes in an actively glaciated basaltic terrain. Earth Planet. Sci. Lett.
843 251, 134–147,
844 Pogge von Strandmann, P.A.E., Burton, K.W., Opfergelt, S., Eiriksdottir, E.S.,
845 Murphy, M.J., Einarsson, A. and Gislason, S.R. (2016) The effect of hydrothermal
846 spring weathering processes and primary productivity on lithium isotopes: Lake
847 Myvatn, Iceland. Chem. Geol. in press, 10.1016/j.chemgeo.2016.02.026I.
848 Pogge von Strandmann, P.A.E., Elliott, T., Marschall, H.R., Coath, C., Lai, Y.J.,
849 Jeffcoate, A.B. and Ionov, D.A. (2011) Variations of Li and Mg isotope ratios in
850 bulk chondrites and mantle xenoliths. Geochim. Cosmochim. Acta 75, 5247–
851 5268,
852 Pogge von Strandmann, P.A.E. and Henderson, G.M. (2015) The Li isotope
853 response to mountain uplift. Geology 43, 67–70,
854 Pogge von Strandmann, P.A.E., Jenkyns, H.C. and Woodfine, R.G. (2013) Lithium
855 isotope evidence for enhanced weathering during Oceanic Anoxic Event 2.
856 Nature Geoscience 6, 668–672,
857 Pogge von Strandmann, P.A.E., Opfergelt, S., Lai, Y.J., Sigfusson, B., Gislason, S.R.
858 and Burton, K.W. (2012) Lithium, magnesium and silicon isotope behaviour
859 accompanying weathering in a basaltic soil and pore water profile in Iceland.
860 Earth Planet. Sci. Lett. 339–340, 11–23,
861 Pogge von Strandmann, P.A.E., Porcelli, D., James, R.H., van Calsteren, P., Schaefer,
862 B.F., Cartwright, I., Reynolds, B.C. and Burton, K.W. (2014) Chemical weathering
863 processes in the Great Artesian Basin: Evidence from lithium and silicon
864 isotopes. Earth Planet. Sci. Lett. 406, 24–36,
865 Rad, S., Rive, K., Vittecoq, B., Cerdan, O. and Allegre, C.J. (2013) Chemical
866 weathering and erosion rates in the Lesser Antilles: An overview in Guadeloupe,
867 Martinique and Dominica. Journal of South American Earth Sciences 45, 331-344,
868 10.1016/j.jsames.2013.03.004I.
869 Rai, S.K., Singh, S.K. and Krishnaswami, S. (2010) Chemical weathering in the
870 plain and peninsular sub-basins of the Ganga: Impact on major ion chemistry and
871 elemental fluxes. Geochim. Cosmochim. Acta 74, 2340–2355,
872 Raymo, M.E. (1994) The Himalayas, organic carbon burial, and climate in the
873 Miocene. Paleoceanography 9, 399-404,
874 Raymo, M.E. and Ruddiman, W.F. (1992) Tectonic Forcing of Late Cenozoic
875 Climate. Nature 359, 117-122,
876 Raymo, M.E., Ruddiman, W.F. and Froelich, P.N. (1988) Influence of late Cenozoic
877 mountain building on ocean geochemical cycles Geology 16, 649-653,
878 Sauzeat, L., Rudnick, R.L., Chauvel, C., Garcon, M. and Tang, M. (2015) New
879 perspectives on the Li isotopic composition of the upper continental crust and its
880 weathering signature. Earth Planet. Sci. Lett. 428, 181–192,
881 Savage, P.S., Georg, R.B., Armytage, R.M.G., Williams, H.M. and Halliday, A.N.
882 (2010) Silicon isotope homogeneity in the mantle. Earth Planet. Sci. Lett. 295,
883 139-146,

884 Sharma, M., Wasserburg, G.J., Hoffmann, A.W. and Chakrapani, G.J. (1999)
885 Himalayan uplift and osmium isotopes in oceans and rivers. Geochim.
886 Cosmochim. Acta 63, 4005-4012,
887 Teng, F.Z., McDonough, W.F., Rudnick, R.L., Dalpe, C., Tomascak, P.B., Chappell,
888 B.W. and Gao, S. (2004) Lithium isotopic composition and concentration of the
889 upper continental crust. Geochim. Cosmochim. Acta 68, 4167–4178,
890 Tomascak, P.B., Langmuir, C.H., Le Roux, P.J. and Shirey, S.B. (2008) Lithium
891 isotopes in global mid-ocean ridge basalts. Geochim. Cosmochim. Acta, 1626-
892 1637,
893 Torres, M.A., West, A.J. and Li, G. (2014) Sulphide oxidation and carbonate
894 dissolution as a source of CO2 over geological timescales. Nature 507, 346–349,
895 Ullmann, C.V., Campbell, H.J., Frei, R., Hesselbo, S.P., Pogge von Strandmann,
896 P.A.E. and Korte, C. (2013) Partial diagenetic overprint of Late Jurassic
897 belemnites from New Zealand: Implications for the preservation potential of
898 d7Li values in calcite fossils. Geochim. Cosmochim. Acta 120, 80–96,
899 Vigier, N., Decarreau, A., Millot, R., Carignan, J., Petit, S. and France-Lanord, C.
900 (2008) Quantifying Li isotope fractionation during smectite formation and
901 implications for the Li cycle. Geochim. Cosmochim. Acta 72, 780–792,
902 Vigier, N., Gislason, S.R., Burton, K.W., Millot, R. and Mokadem, F. (2009) The
903 relationship between riverine lithium isotope composition and silicate
904 weathering rates in Iceland. Earth Planet. Sci. Lett. 287, 434–441,
905 Vigier, N. and Godderis, Y. (2015) A new approach for modeling Cenozoic oceanic
906 lithium isotope paleo-variations: the key role of climate. Climate of the Past 11,
907 635–645,
908 Walker, J.C.G., Hays, P.B. and Kasting, J.F. (1981) A Negative Feedback Mechanism
909 for the Long-Term Stabilization of Earths Surface-Temperature. Journal of
910 Geophysical Research-Oceans and Atmospheres 86, 9776-9782,
911 Wang, Q.-L., Chetelat, B., Zhao, Z.-Q., Ding, H., Li, S.-L., Wang, B.-L., Li, J. and Liu, X.-
912 L. (2015) Behavior of lithium isotopes in the Changjiang River system: Sources
913 effects and response to weathering and erosion. Geochim. Cosmochim. Acta 151,
914 117–132,
915 Wanner, C., Sonnenthal, E.L. and Liu, X.-M. (2014) Seawater δ7Li: A direct proxy
916 for global CO2 consumption by continental silicate weathering? Chem. Geol. 381,
917 154–167,
918 West, A.J. (2012) Thickness of the chemical weathering zone and implications for
919 erosional and climatic drivers of weathering and for carbon-cycle feedbacks.
920 Geology, 10.1130/G33041.1I.
921 West, A.J., Bickle, M.J., Collins, R. and Brasington, J. (2002) Small-catchment
922 perspective on Himalayan weathering fluxes. Geology 30, 355–358,
923 West, A.J., Galy, A. and Bickle, M. (2005) Tectonic and climatic controls on silicate
924 weathering. Earth Planet. Sci. Lett. 235, 211–228,
925 Williams, L.B. and Hervig, R.L. (2005) Lithium and boron isotopes in illite-
926 smectite: The importance of crystal size. Geochim. Cosmochim. Acta 69, 5705-
927 5716,
928 Wimpenny, J., Gislason, S.R., James, R.H., Gannoun, A., Pogge von Strandmann,
929 P.A.E. and Burton, K.W. (2010a) The behaviour of Li and Mg isotopes during
930 primary phase dissolution and secondary mineral formation in basalt. Geochim.
931 Cosmochim. Acta 74, 5259-5279,

932 Wimpenny, J., James, R.H., Burton, K.W., Gannoun, A., Mokadem, F. and Gislason,
933 S.R. (2010b) Glacial effects on weathering processes: New insights from the
934 elemental and lithium isotopic composition of West Greenland rivers Earth
935 Planet. Sci. Lett. 290, 427-437,
936 Witherow, R.A., Berry Lyons, W. and Henderson, G.M. (2010) Lithium isotopic
937 composition of the McMurdo Dry Valleys aquatic systems. Chem. Geol. 275, 139–
938 147,
939 Wunder, B., Meixner, A., Romer, R.L. and Heinrich, W. (2006) Temperature-
940 dependent isotopic fractionation of lithium between clinopyroxene and high-
941 pressure hydrous fluids. Contrib. Mineral. Petrol. 151, 112-120,
942 Ziegler, K., Chadwick, O.A., Brzezinski, M.A. and Kelly, E.F. (2005) Natural
943 variations of delta Si-30 ratios during progressive basalt weathering, Hawaiian
944 Islands. Geochim. Cosmochim. Acta 69, 4597-4610,
945

946

947

948

949

950

951

Sample	River	Degrees North	Degrees East	Altitude (m)	Li (ng/ml)	δ^7Li	2sd	Sil w.r. (t/km^2/yr)
1	Bhagirathi	30.156	78.603	648	3.23	10.9	0.9	
2	Alaknanda	30.145	78.601	476	2.29	10.7	0.5	
4	Ganga	30.127	78.354	353	3.03	12.9	0.1	8.37
5	Yamuna	28.748	77.226	210	6.65	22.0	0.4	10.3
6	Ganga	28.827	78.154	205	7.10	17.5	0.3	
7	Ramganga	28.666	78.896	185	6.03	23.0	1.0	
8	Unnamed Trib to Ganga	28.031	78.780	170	11.7	23.5	0.8	
9	Ganga	27.930	78.858	165	7.03	16.4	0.2	
10	Yamuna	27.177	78.043	157	10.8	18.4	0.1	
11	Unnamed Trib to Yamuna	26.963	78.365	142	7.60	21.6	0.5	
12	Chambal	26.870	78.367	138	6.72	18.9	0.2	
13	Yamuna	26.602	79.119	113	9.51	19.9	0.2	
14	Chambal	26.549	79.088	125	6.50	19.3	0.8	4.89
15	Unknown Trib to Chambal	26.435	79.209	105	9.29	20.3	0.1	
16	Yamuna	26.425	79.246	105	7.63	22.0	0.2	
17	Ganga	27.010	79.987	127	6.45	21.9	0.1	
18	Unnamed Trib to Ganga	27.271	79.949	133	6.58	16.8	0.3	
19	Ramganga	27.498	79.696	137	6.13	24.8	0.6	19.1
20	Ganga	27.399	79.628	138	6.95	20.6	0.1	

21	Ganga	26.438	80.412	116	5.95	19.4	0.7	
22	Yamuna	25.955	80.160	110	7.59	22.1	0.7	
23	Betwa	25.944	80.156	107	5.52	20.8	0.1	5.09
24	Unnamed Trib to Yamuna	25.654	80.148	111	7.60	19.4	0.9	
25	Ken	25.480	80.313	96	4.61	22.5	0.2	6.39
26	Yamuna (South)	25.708	80.604	87	6.55	21.0	0.8	
27	Yamuna (North Bank)	25.714	80.607	87	6.68	21.5	0.6	
28	Yamuna	25.425	81.882	87	6.14	21.3	0.1	6.87
29	Ganga	25.427	81.887	86	6.39	19.1	0.5	
30	Tons	25.243	82.041	72	5.20	20.3	0.5	3.56
31	Ganga	25.309	82.076	89	6.35	20.9	0.6	
33	Ganga	25.152	82.546	64	5.60	20.2	0.2	
34	Varuna	25.341	82.981	71	6.41	20.0	0.2	
35	Ganga	25.290	83.006	82	6.53	21.2	0.1	
36	Gomati	25.506	83.142	66	6.32	21.4	0.3	5.84
37	Ganga	25.501	83.168	75	6.72	20.9	0.5	
38	Ganga	25.535	83.215	61	2.96	20.6	0.3	
39	Ganga	25.679	84.719	60	6.25	21.2	0.3	
40	Son	25.564	84.790	65	0.43	21.9	0.5	5.17
41	Ghaghara	25.821	84.590	61	6.01	20.9	0.8	6.63
42	Ganga	25.730	84.829	62	2.39	20.7	0.5	
43	Gandak	25.702	85.198	57	3.42	16.7	0.4	9.85
44	Ganga	25.615	85.201	52	2.00	21.7	1.0	
45	Ganga	25.381	86.001	49	2.32	20.8	0.6	
46	Unknown Trib to Ganga	25.502	86.481	42	1.64	21.7	1.0	2.31
47	Innundated Area	25.406	86.779	36	1.09	20.2	0.6	
48	Kosi	25.424	87.235	31	1.58	24.6	0.4	9.34
49	Ganga	25.282	87.248	40	2.23	20.9	0.2	
50	Ganga	24.801	87.948	27	1.66	22.1	0.1	
51	Hooghly	22.651	88.351	7	1.66	20.6	0.3	

952

953 Table 1. Dissolved load Li isotope ratios and silicate weathering rates. See Frings
954 et al. (2015) for major and trace element concentrations. “2sd” refers to the 2
955 standard deviations of multiple analyses of the same solution (generally n=3).

956

Sample	Position	Depth (m)	δ^7Li	2sd
1	Surface	0	-1.6	0.1
2	Surface	0	0.1	0.1
14	Bank		0.2	0.1
28	Shallow	0	-0.6	0.6
28	Deep	-	-1.3	0.7

40	Shallow	0	-2.6	0.6
40	Deep	3	2.9	0.6
41	Shallow	0	-0.1	0.6
41	Medium	5	0.1	0.6
41	Deep	9	0.0	0.5
49	Shallow	0	-0.4	0.2
49	Deep	10	0.1	0.2

Table 2. Sediment Li isotope ratios. Sample locations are the same as for Table 1.

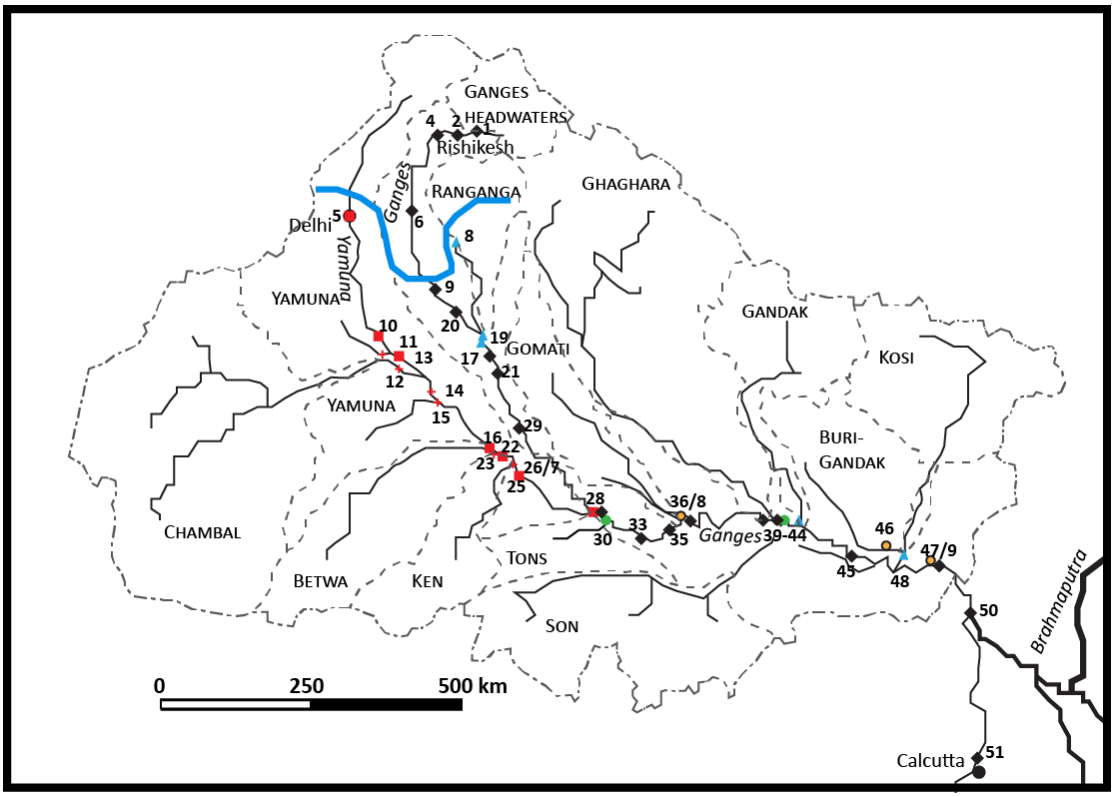

Figure 1. Sample location map, modified from Frings et al. (2015). The dotted grey lines show the individual catchment areas. The sample location symbols are the same as those used in Figures 2 and 8. The blue curved line shows the location below which the floodplain is at steady-state according to dissolved Li isotopes (see text for details).

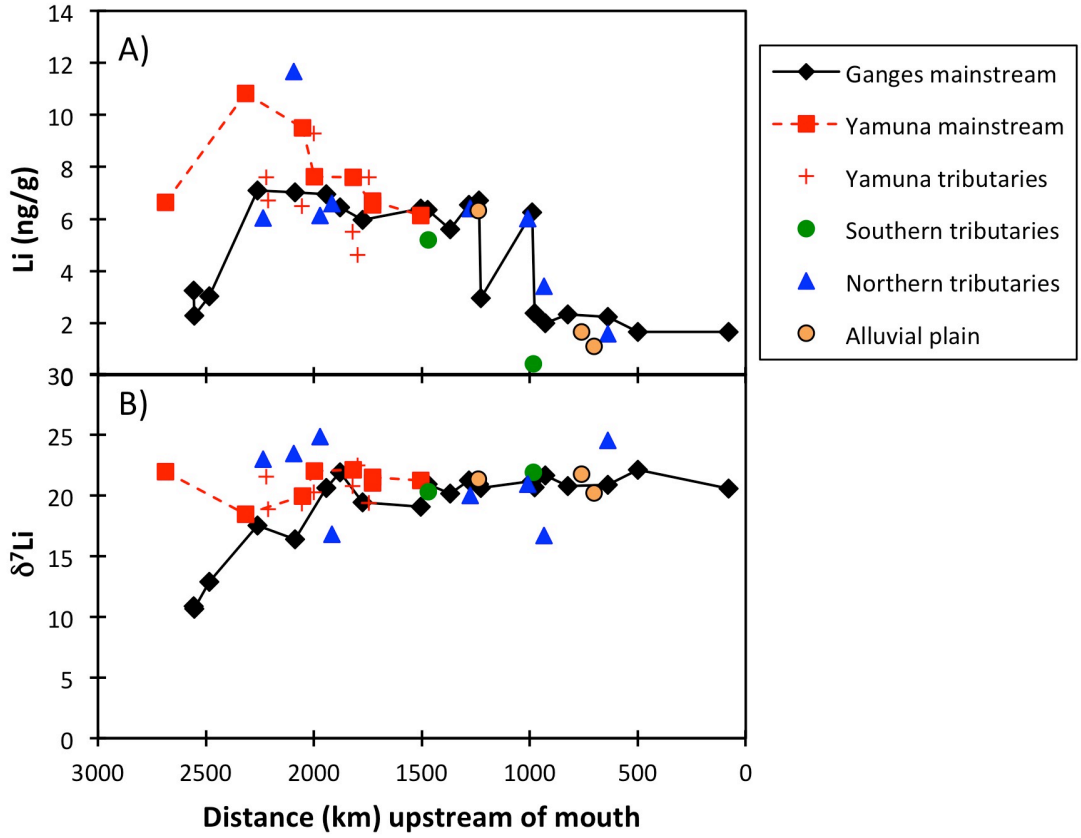

968

969 Figure 2. Comparison of the Li concentration (A) and isotope ratio (B) to flow

970 distance upstream from the river mouth for the Ganges and its tributaries.

971

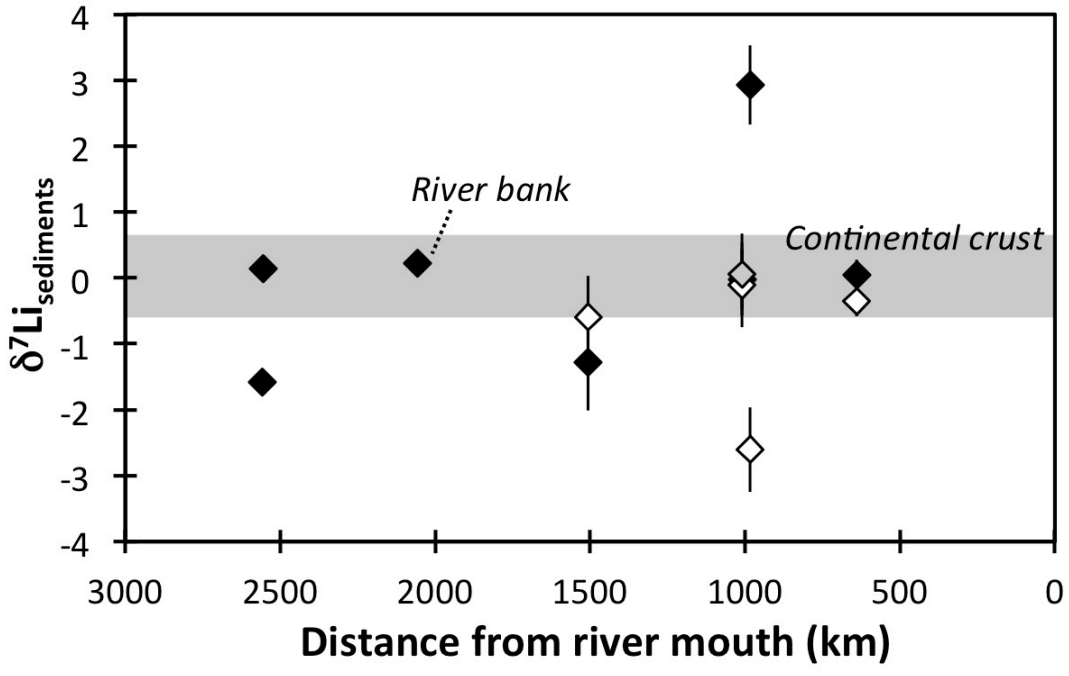

972

973 Figure 3. Li isotope ratio of river sediments plotted as a function of flow distance
974 above the river mouth. Open diamonds are shallow samples from the river flow,
975 filled grey symbol is medium depth, and black symbols are deeper samples. The
976 grey bar is the mean continental crust (Sauzeat et al., 2015).
977

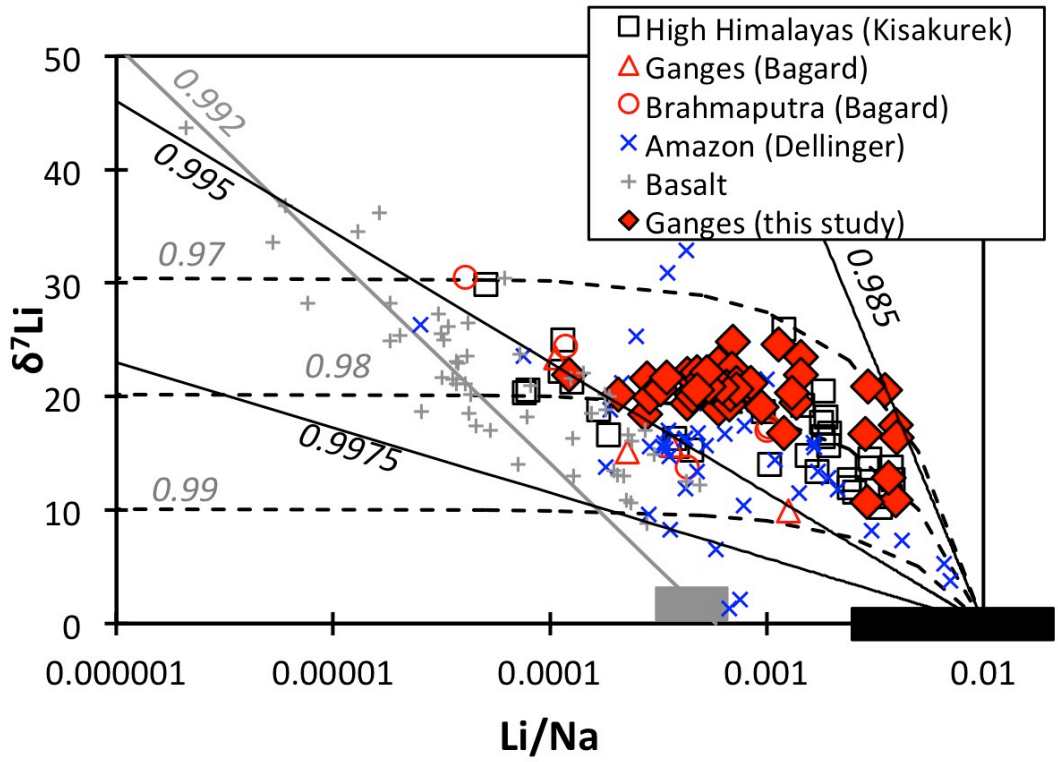

978

979 Figure 4. Dissolved Li/Na mass ratios plotted against δ^7Li for this study, the High
980 Himalayas (Kisakürek et al., 2005), the Ganges-Brahmaputra (Bagard et al.,
981 2015), the Amazon (Dellinger et al., 2015) and basalts from Iceland, the Azores
982 and the Columbia River Basalts (Liu et al., 2015; Pogge von Strandmann et al.,
983 2010; Pogge von Strandmann et al., 2006; Vigier et al., 2009). The solid lines are
984 Rayleigh fractionation relationships (see text for details), the dashed lines are
985 Batch fractionation relationships and the associated numbers the isotopic
986 fractionation factors (black for Rayleigh, grey for Batch). The black box

represents the range of Li/Na from river sediments from the Amazon and Ganges, as well as global shales (Dellinger et al., 2014). The grey line is a Rayleigh relationship for basaltic terrains, using the grey box as a starting composition (Pogge von Strandmann et al., 2010; Pogge von Strandmann et al., 2006). Dissolved load values have been corrected for precipitation input when data have been provided, otherwise are uncorrected.

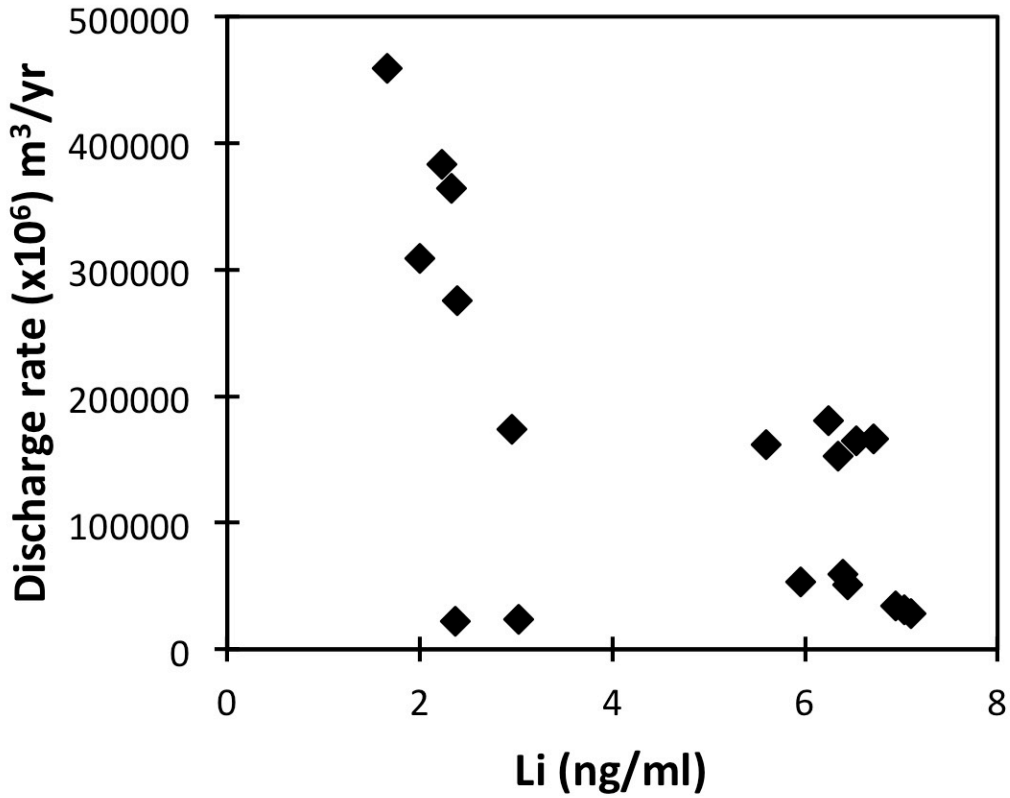

Figure 5. Li concentrations plotted against discharge rates. Samples are unaffected by dilution, except potentially those with highest discharge, which are those close to the Ganges mouth and have constant δ^7Li.

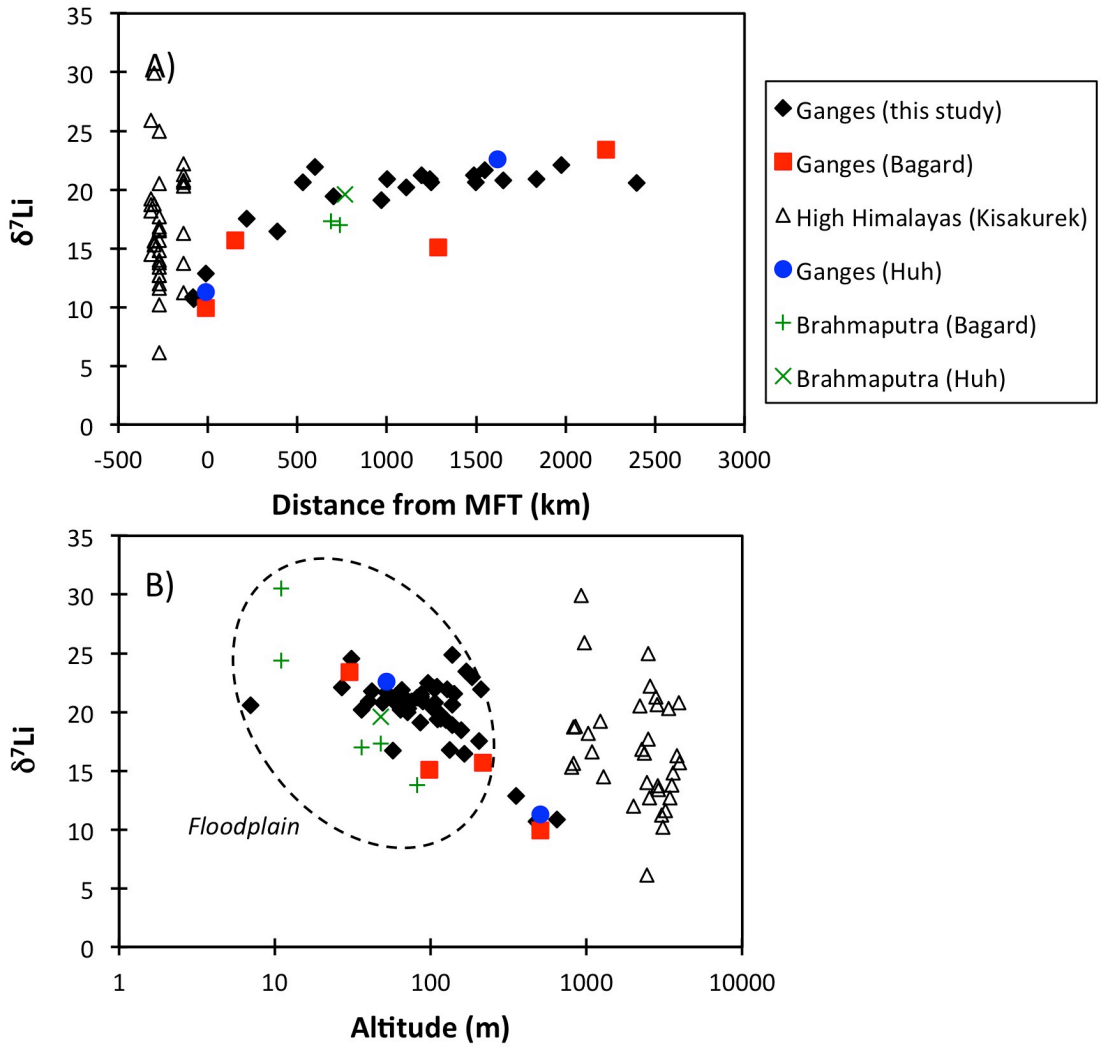

999

1000 Figure 6. A) Dissolved Li isotope ratios for all studies of the Ganges-Brahmaputra
1001 rivers system, plotted against distance from the Main Frontal Thrust (MFT) that
1002 delineates the edge of the high relief areas (Bagard et al., 2015; Huh et al., 1998;
1003 Kisakürek et al., 2005), showing the unchanging nature of δ^7Li in the Ganges over
1004 at least 3 decades. Only rivers that actually cross the MFT are plotted. Distances
1005 for the Kisakurek et al. (2005) rivers were measured using Google Maps. B) The
1006 same data plotted against altitude, as an approximation of uplift and exposure
1007 rates. Samples from south of the MFT are considered floodplain samples.

1008

1009

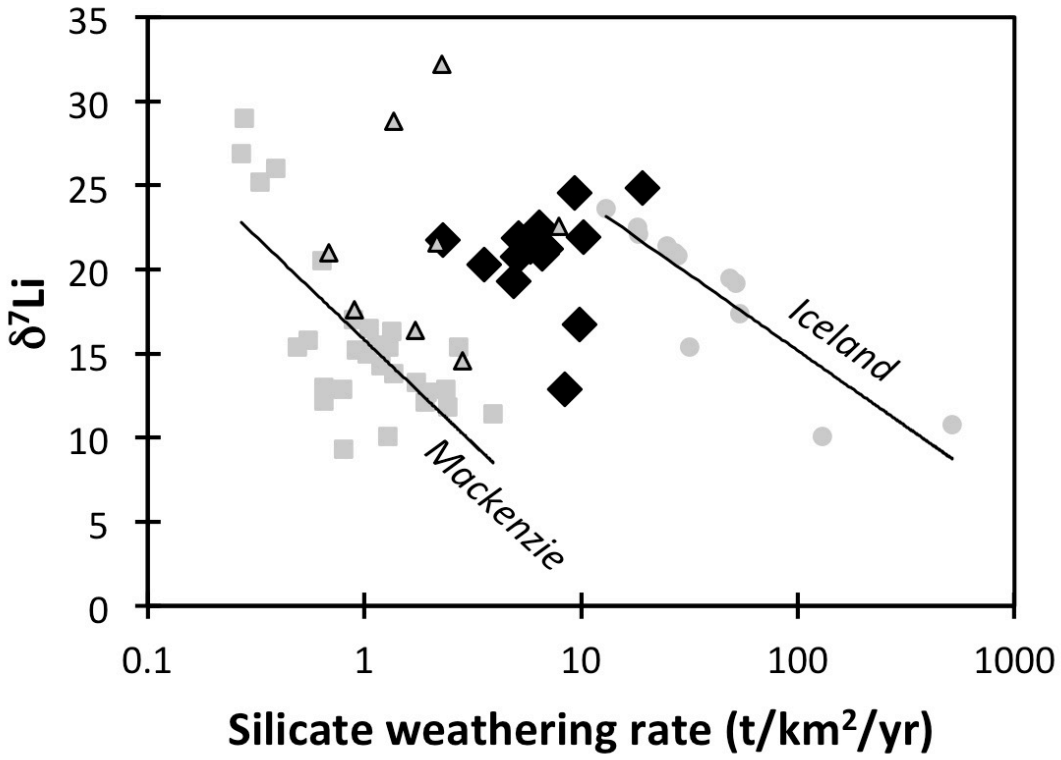

Figure 7. Riverine Li isotopes plotted as a function of the silicate weathering rate. While there are correlations between the two parameters for two relatively small river systems (Iceland and the Mackenzie River (Millot et al., 2010; Vigier et al., 2009)), there is not correlation for large global rivers (triangles (Huh et al., 1998)), or for the Ganges (this study – black diamonds) which are responsible for >30% of the global riverine discharge into the oceans. Lithium isotopes are therefore clearly not a weathering-rate tracer, and cannot be used as such in the palaeo-record.

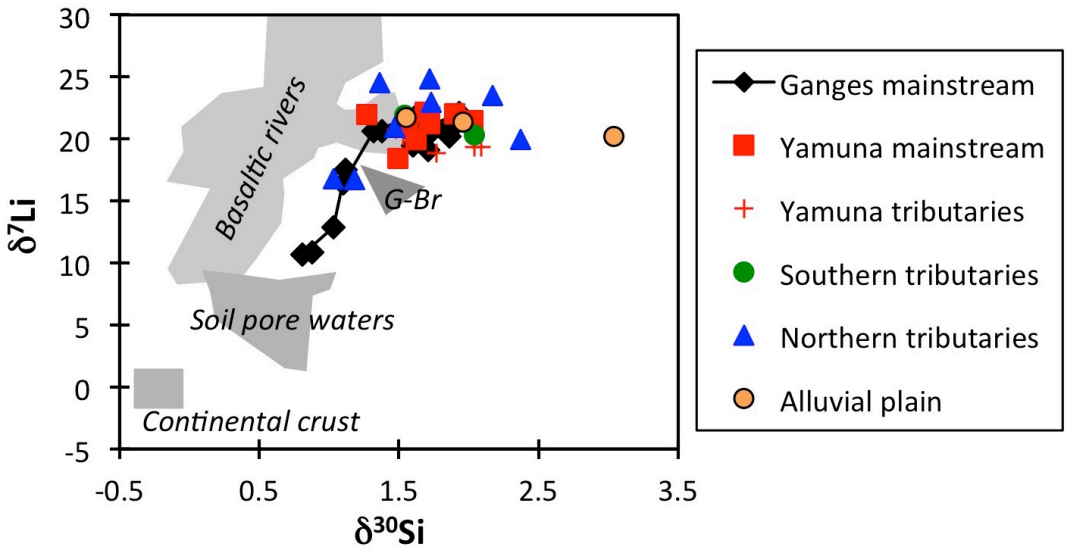

1022

1023 Figure 8. Li isotopes plotted against Si isotopes (Frings et al., 2015) for the
1024 Ganges river system. The Ganges mainstream exhibits a positive correlation,
1025 which most other samples do not. In comparison, a few points from a previous
1026 Ganges-Brahmaputra (G-Br) study are shown (Bagard et al., 2015; Georg et al.,
1027 2009). Some basaltic rivers also exhibit a Li-Si co-variation (Opfergelt et al.,
1028 2013), while neither some other Icelandic rivers (Georg et al., 2007; Vigier et al.,
1029 2009), nor Icelandic soil pore waters exhibit a co-variation (Pogge von
1030 Strandmann et al., 2012). Average upper continental crust values are from
1031 Sauzeat et al., 2015; Savage et al., 2010.

1032

1033

1034